Article

Constant Speed Control of Hydraulic Travel System Based on Neural Network Algorithm

Haoyun Ye [ID], Xiangdong Ni *, Huajun Chen [ID], Daolin Li and Wenlong Pan

College of Mechanical and Electrical Engineering, Shihezi University, Xinjiang Uygur Autonomous Region, Shihezi 832003, China; lucky_yhy2022@163.com (H.Y.); jun_9004@163.com (H.C.); li13279256824@163.com (D.L.); panwenlong6666@163.com (W.P.)
* Correspondence: nini0526@126.com

Abstract: In order to solve the problems of poor stability of the output speed and poor synchronization of the pump-controlled dual motor in a hydraulic travel system during step input speed and external load disturbance, different control strategies were designed and compared with the state machine using the statechart module control, Z-N frequency response PID control, and GA-based PID parameter self-tuning methods. Our analysis shows that the BP algorithm-based PID parameter self-tuning control method has no overshoot and that the three methods reduced the target speed tracking time by 90.11%, 75.12% and 36.55%, respectively. The average synchronous error for the system output speed was 7.95%. The stability and synchronization requirements of the constant speed of the hydraulic travel system were satisfied. These research results can provide a reference for the design and application of constant speed control for pump-controlled dual-motor hydraulic travel systems in the fields of engineering and agricultural machinery.

Keywords: hydraulic travel system; speed control; neural network algorithm; synchronous control

1. Introduction

Hydraulic travel systems have the characteristics of high power density and reliable operation, and are mainly used in the transmission systems of large and medium-sized construction machinery and vehicles [1,2]. The variable pump-controlled motor in the system is the speed-regulating mechanism of the hydraulic system and energy transfer is carried out through flow and pressure [3]. The system can achieve automatic matching of the pump output with the external load through the regulating action of the controller, thus the flow coming from the pump output is essentially input to the motor, which is combined with the gearbox in a different way and is able to achieve step-less speed change through hydraulic step-less speed regulation [4,5]. The characteristics of the speed control mechanism of the hydraulic travel system greatly affect the speed control performance of the vehicle transmission [6]. Therefore, the study of the speed regulation characteristics of hydraulic travel systems is of great significance for the study of hydraulic vehicle transmissions.

Extensive domestic and foreign research has been carried out into constant speed control methods for hydraulic travel systems [7]. Ayad Q. Hussien used PI (proportional and integral) and FL (fuzzy logic) controllers to simulate the angular velocity of the hydraulic motor of the pump-controlled motor system [8]. N Kumar [9,10] et al. studied a hydraulic closed loop drive system with steady-state performance. Their experimentally proposed drive system consisted of a variable displacement pump and a bent shaft motor. The performance of two different constant speed operation modes, single motor drive and dual motor drive, was investigated. The speed control strategy of the quantitative pump-variable motor system studied by Kou Mingkun [11,12] had a more detailed control effect on a single pump and a single motor. However, most scholars [13,14] have only analyzed the output speed control method of single-pump single motor hydraulic speed

control systems, and the research on single-pump double motor constant speed systems is relatively deficient.

This paper takes a hydraulic travel system with a single pump and two motors as the research object, and on the basis of establishing its mathematical model proposes a variety of different control strategies for analysis and comparison in order to study the effect of constant speed control of the motor under step input speed and external load disturbance and to improve the synchronization and stability of the hydraulic travel system.

2. Hydraulic Travel System Working Principle

The closed-circuit hydraulic system is shown in Figure 1; it consists of a variable hydraulic pump and two variable displacement piston motors (one front and one rear), an electro-hydraulic proportional variable mechanism, hydraulic valves, and other components. The front drive motor is mounted directly on the gearbox, while the rear drive motor is mounted directly on the rear gearbox. The displacement of the hydraulic pump and the motor is changed, which in turn controls the motor speed synchronously, thus controlling the vehicle's driving speed.
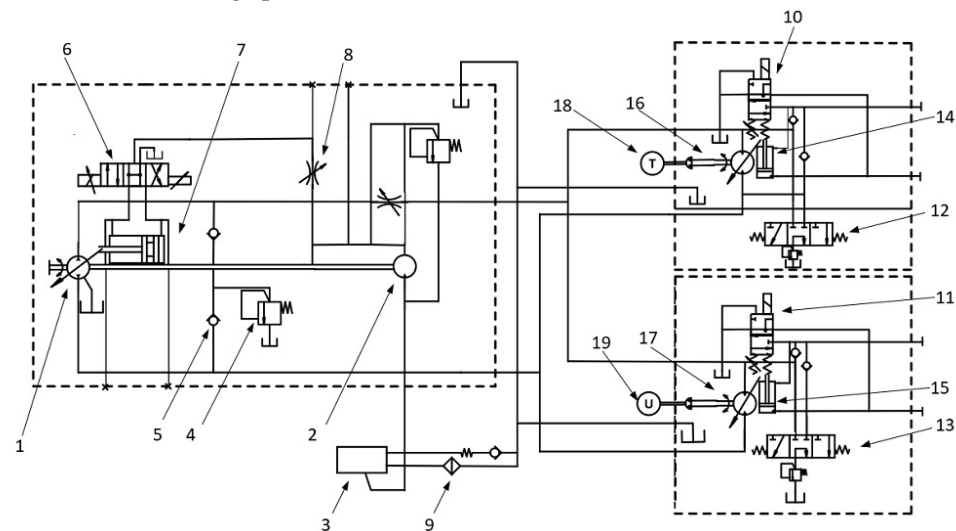

Figure 1. Transmission principle diagram of hydraulic traveling system. 1. Hydraulic pump; 2. Charge pump; 3. Hydraulic oil tank; 4. Pressure regulating valve; 5. Check valve; 6. Hydraulic pump solenoid valve; 7. Hydraulic pump cylinder; 8. Throttle valve; 9. Hydraulic oil cooler; 10. Front hydraulic motor solenoid valve; 11. Rear hydraulic motor solenoid valve; 12. Front hydraulic flow regulating solenoid valve; 13. Rear hydraulic flow regulating solenoid valve; 14. Front motor hydraulic cylinder; 15. Rear motor Hydraulic cylinder; 16. Front hydraulic motor; 17. Rear hydraulic motor; 18. Gearbox; 19. Rear gearbox.

As shown in Figure 2, the difference between the actual speed of the motor and the target speed is converted into an electrical signal by the controller and input to the electro-hydraulic proportional variable mechanism, which then changes the swash plate tilt angle of the variable pump to adjust the variable pump displacement ratio, thus controlling the motor speed. During operation, the cross-coupling controller makes the difference between the angular velocities of the two channel motor outputs; the difference is used as the output of the cross-coupling controller, multiplied by the corresponding adjustment factors Gain1 and Gain2, then input to the two motors in order to control the two channels of the motors equally and improve their synchronization.

Figure 3 shows a block diagram of the mathematical model of the hydraulic travel system, with the meanings of the parameters shown in Table 1. In Figure 3, the deviation value obtained from the input voltage $U(s)$ and the feedback voltage $U_f(s)$ is used as the input value of the system; the block diagram of the pump-controlled motor transfer function of the hydraulic system can be obtained after the proportional amplifier K_α, electro-

hydraulic proportional directional valve K_{bv}, valve-controlled cylinder, etc. $T_L(s)$ is the disturbing load outside the system and $\theta_m(s)$ is the motor's output speed. The open-loop transfer function of the hydraulic speed control system is

$$G(s) = \frac{K_{fv}}{s(\frac{1}{\omega_h^2}s^2 + \frac{2\delta_h}{\omega_h}s + 1)} \tag{1}$$

where $K_{fv} = \frac{K_\alpha K_{bv} K_q K_\phi K_{qp} K_f}{A D_m}$ is the open-loop gain of the system, K_α is the proportional amplification gain coefficient, K_{bv} is the proportional valve gain coefficient, K_q is the valve stable operating point flow gain coefficient, K_Φ is the variable pump swash-plate tilt angle coefficient, K_{qp} is the variable pump flow gain, K_f is the speed sensor gain coefficient, A is the effective area of the hydraulic cylinder piston, D_m is the motor displacement, ω_h is the system is the inherent frequency of the system, and δ_h is the damping ratio of the system.
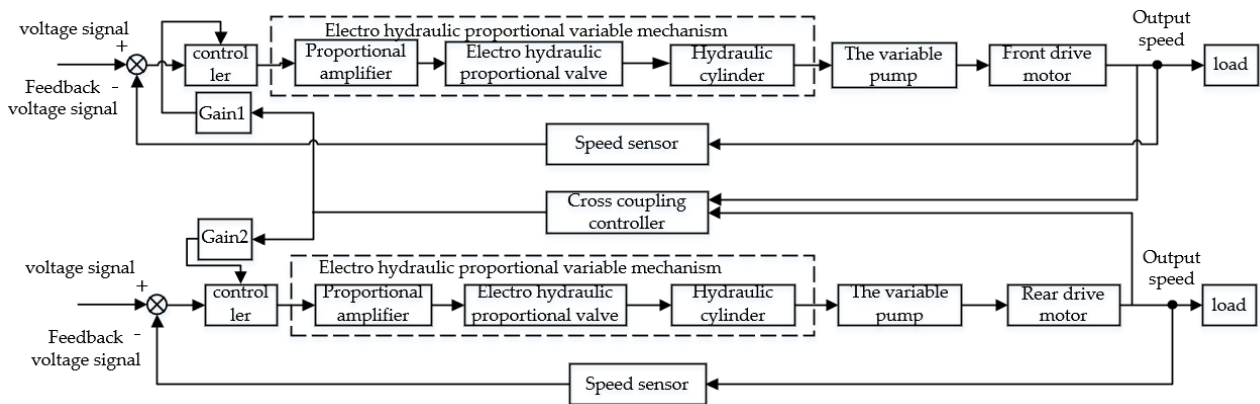

Figure 2. Speed regulation principle of hydrostatic travel system.
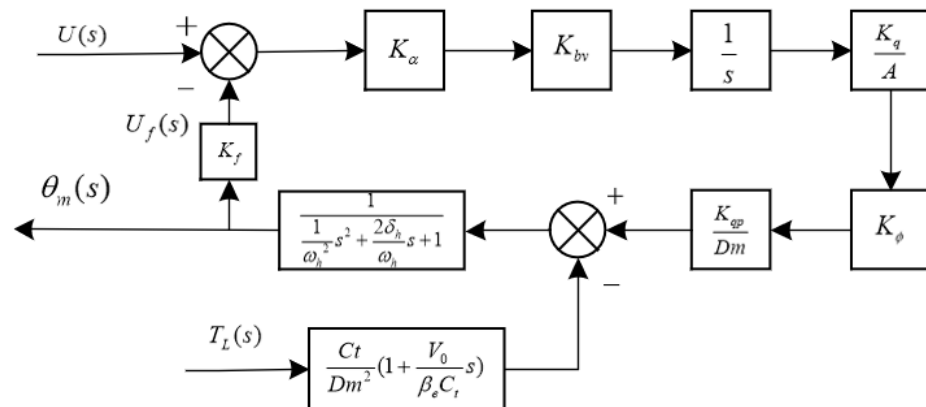

Figure 3. Block diagram of the mathematical model of pump-controlled motor.

By consulting the parameter indicators of each component in the hydraulic speed control system and substituting them into Equation (1), the third-order open-loop transfer function of the hydraulic speed control system can be obtained as shown in the equation below.

Hydraulic travel system front drive motor transfer function:

$$G(s) = \frac{62.19}{1.29 \times 10^{-4}s^3 + 4.9 \times 10^{-3}s^2 + s} \tag{2}$$

Hydraulic travel system rear drive motor transfer function:

$$G_1(s) = \frac{93.073}{2.89 \times 10^{-4}s^3 + 1.32 \times 10^{-2}s^2 + s} \tag{3}$$

When the open-loop frequency characteristics of the hydraulic travel system are analyzed, the condition of the system's stability is that the amplitude margin is smaller than the phase margin; as can be seen from Figure 4, the amplitude margin of the front drive motor traverses the frequency of 88.0019 rad/s and the phase margin traverses the frequency of 88.1052 rad/s, while the amplitude margin of the rear drive motor traverses the frequency of 75.2332 rad/s and the phase margin traverses the frequency of 61.7190 rad/s. The amplitude margin and phase margin traversal frequency of the front drive motor are very close, while the amplitude margin traversal frequency of the rear drive motor is 75.2332 rad/s, > the phase margin of 61.7190 rad/s; thus, it can be seen that the system is less stable and the tracking performance is not good.

Table 1. Parameters of pump-controlled motor mathematical model.

Parameter	Symbol	Unit	Parameter	Symbol	Unit
Proportional amplification gain	K_α	A/V	Rear motor displacement	D_{m2}	m³/rad
Proportional valve gain coefficient	K_{bv}	N/A	System natural frequency	ω_h	rad/s
Flow gain at stable operating point of valve	K_q	m²/s	System damping ratio	δ_h	——
Effective area of hydraulic cylinder piston	A	m²	Total leakage coefficient of pump and motor	C_t	m⁵/N·s
Variable displacement pump swash-plate inclination coefficient	K_Φ	rad/m	Effective volume of hydraulic circuit	V_0	m³
Variable pump flow gain	K_{qp}	m²/s	Effective bulk modulus of elasticity	β_e	N/m
Front motor displacement	D_{m1}	m³/rad	Speed sensor gain factor	K_f	V·s/rad

(**a**) Bode diagram of open loop characteristics of rear drive motor

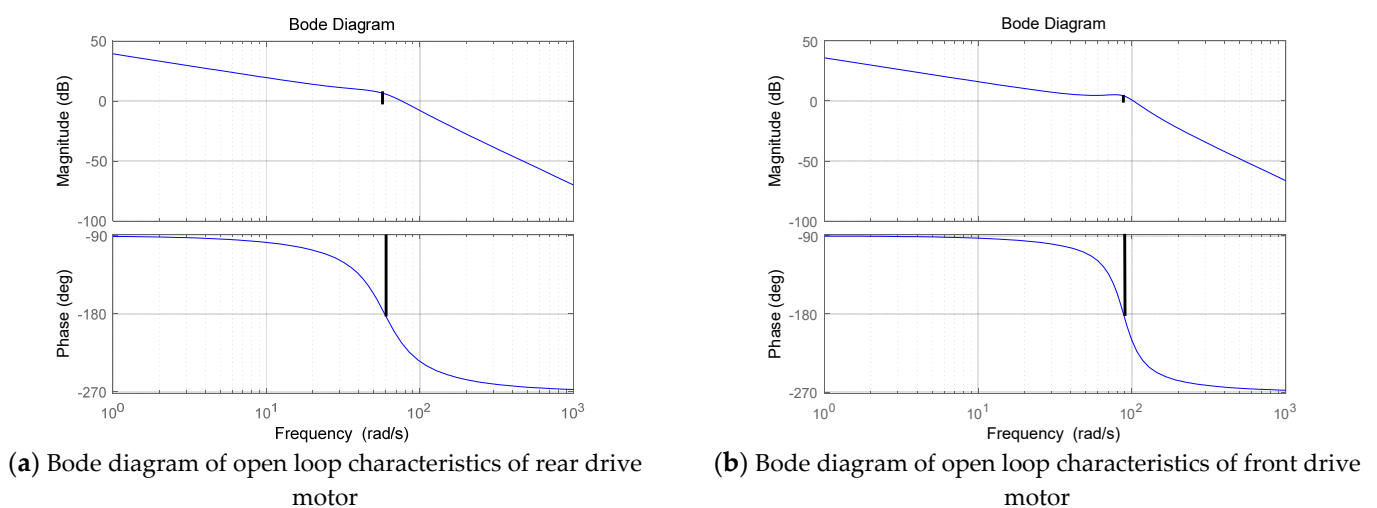(**b**) Bode diagram of open loop characteristics of front drive motor

Figure 4. Bode diagram of the open-loop frequency characteristics of the system.

3. Rotational Speed Adaptive Tracking Controller Design

In order to solve the problems of poor stability of the output speed and poor synchronization of the pump-controlled dual motor in the hydraulic travel system under step input speed and external load disturbance, different control strategies were used to design a

constant speed controller for the hydraulic travel system. First, the system transfer function was derived from the mathematical model of the hydraulic travel system; on the basis of the mathematical model, the simulation model of the hydraulic travel system was built and the model-based controller design was carried out using MATLAB\Simulink simulation software (Simulink being an important part of MATLAB). Simulink can develop complex control structures through multi-domain simulation and is a block diagram environment for model-based controller design. Second, the hydraulic travel system was built in Simcenter Amesim simulation software and the controller part of the system was designed using a state machine with the statechart module in Simcenter Amesim simulation software, which is a powerful system simulation software of LMS and can realize simulation calculations in the mechanical, hydraulic, and electrical fields. The state machine used with the statechart module in Simcenter Amesim software is a control module for creating monitoring programs, defining scenarios, or creating any type of conditional or event-based logic. Finally, after comparing and analyzing different simulation software and different control strategies, the optimal method for constant speed control of the hydraulic travel system was derived and the optimal controller for constant speed control of the hydraulic travel system was designed to finally achieve synchronous and constant control of the system output speed under step input and external load disturbance conditions.

3.1. Design of Hydraulic Travel Control System in Simcenter Amesim

Using Simcenter Amesim simulation software, the controller was designed by using a state machine with the statechart module. The state machine control module describes a set of connection states which can be activated when specific conditions are met. This is a convenient way to build monitors, define scenarios, or create any type of conditional or event-based logic. The model is shown in Figure 5. Closed-loop control with state machine module control and motor speed feedback was used in the model and a speed sensor was used to feed the vehicle speed back to the controller, creating external closed-loop feedback to achieve control of the motor speed.
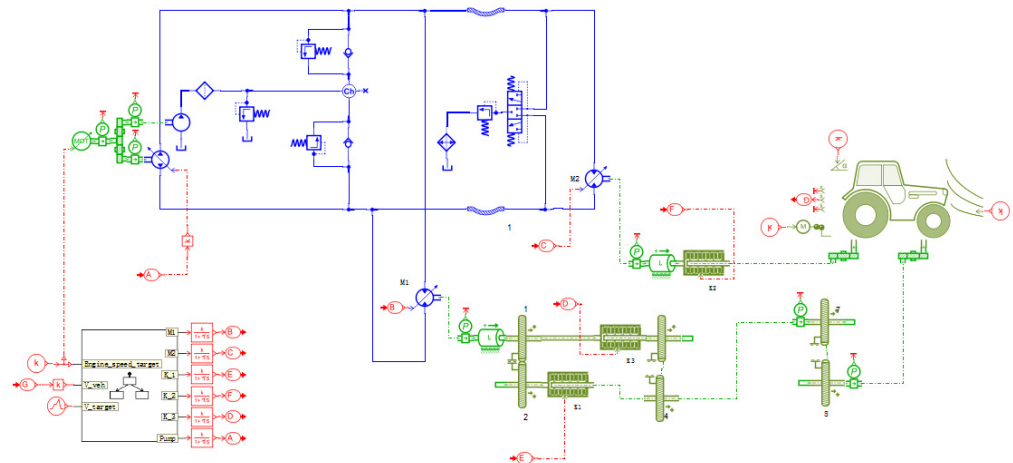

Figure 5. Model of hydraulic travel system based on state machine control.

3.2. Overall Design of the Controller in Simulink

In the complex and changing working environment of construction machinery, construction machinery systems often face situations where the engine speed and load working conditions change, seriously affecting the working performance of the system. How to maintain the motor output speed at a constant level despite the frequent changes of external disturbances is a prominent problem facing construction machinery [15,16] For the hydraulic speed control system, step input speed and output speed instability are caused by external load disturbance; in addition, the dual motors are not synchronized, and there are other problems as well. As shown in Figure 6, the control variables obtained from the

output speed ω_1, ω_2 through the cross-coupled controller are passed to the internal system controller again through the gain coefficients *K1*, *K2*, respectively, in order to achieve closed-loop feedback control. In the external feedback link, the deviations of the output speed ω_1, ω_2 and the target input speed ω are passed to the internal system controller and the system forms a closed-loop control internally and externally. Thus, four different control strategies were designed to derive the control strategy most applicable to the constant speed adaptive hydraulic travel system, and the dynamic characteristics of the hydraulic travel system were brought as close as possible to a known reference model by designing an adaptive algorithm to improve the system's stability and robustness. When driving in a straight line, n_1, n_2, and n_k are specified as the speed and speed difference of the walking hydraulic motors on both sides, respectively, and *e* is specified as its error allowance in straight line driving; when n_k is less than *e*, the controller does not make any response, while when n_k is greater than *e* the controller executes the double closed-loop straight line driving control program. The logic design flow chart is shown in Figure 7.
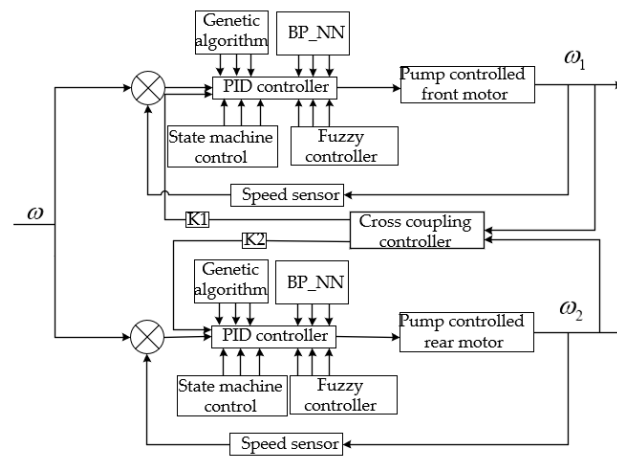

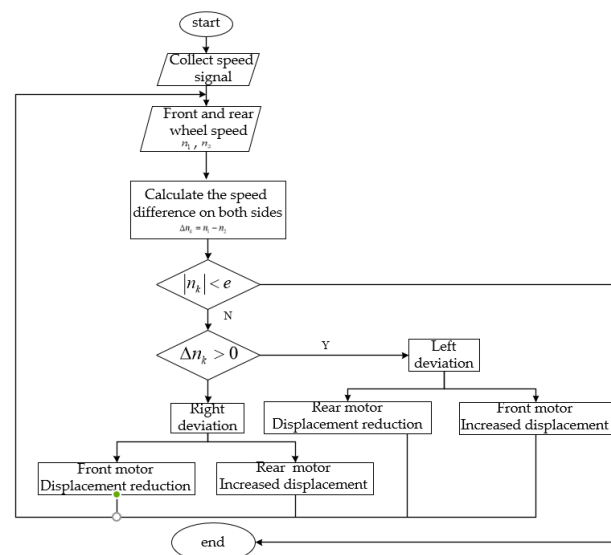**Figure 6.** System adaptive tracking control framework.

Figure 7. Flow chart of motor synchronous driving control.

3.2.1. Design of PID Controller Based on Z–N Frequency Response

In practical engineering, the most widely used regulator control law for proportional integral differential control is referred to as PID (Proportion Integration Differentiation) control, known as PID regulation. It has become one of the main technologies of industrial control thanks to its simple structure, good stability, reliable work, and easy adjustment.

The Ziegler–Nichols frequency tuning method adjusts the PID parameters according to the frequency response in order to specify the proportional parameter, K_p, integral parameter, K_i, and differential parameter, K_d, during the tuning process to regulate the dynamic process response time. The MATLAB program was used to implement the Z–N algorithm; the controller model was built as shown in Figure 8 by specifying the controlled object transfer function and obtaining the corresponding root trajectory through the corresponding j_w axis point with the gain coefficient K_r and ω_r; its rectification equation is

$$K_p = 0.6K_r, K_i = \frac{K_p\omega_r}{\pi}, K_d = \frac{K_p\pi}{4\omega_r} \tag{4}$$

where K_r is the gain value of the system with periodic oscillation, ω_r is the oscillation frequency, K_p is the proportional parameter of the PID controller, K_i is the integral parameter of the PID controller, and K_d is the differential parameter of the PID controller.
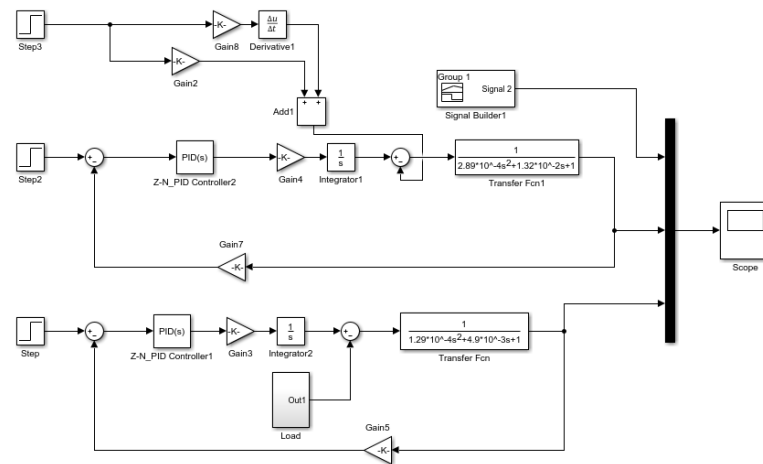

Figure 8. Ziegler-Nichols frequency tuning PID simulation model.

Figure 9 shows the hydraulic travel system rear drive motor system. After adjustment, the amplitude margin crossing frequency $\omega_c <$ the phase margin crossing frequency ω_g. It can be seen that the Ziegler–Nichols frequency adjustment method for adjusting PID parameter values meets the design requirements. According to the PID adjustment formula, $K_p = 0.0894$, $K_i = 1.4969$, and $K_d = 0.0013$, while the hydraulic travel system front drive motor system PID adjustment results are $K_p = 0.0925$, $K_i = 0.0800$, and $K_d = 0.0800$.
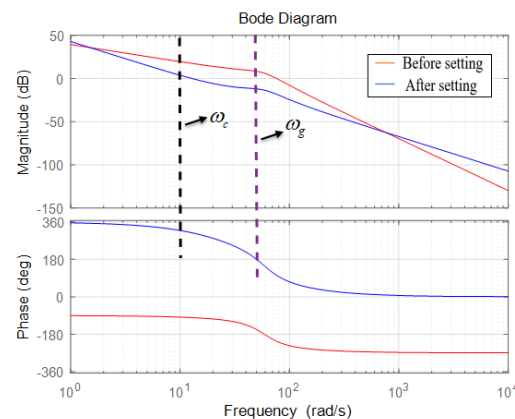

Figure 9. System bode diagram before and after Ziegler-Nichols frequency setting.

3.2.2. Design of Fuzzy PID Controller

In this paper, we chose a two-input, three-output, Mamdani-type fuzzy controller, where the input is the deviation e of the actual motor speed value from the motor target

speed value and the deviation rate of change *ec*, and the output is ΔK_p, ΔK_i, ΔK_d. The fuzzy domain of the controller input variables *e*, *ec* and output quantities ΔK_p, ΔK_i, ΔK_d are {−3,3}. Let the fuzzy subsets of input quantities *e*, *ec*, and output quantities ΔK_p, ΔK_i, and ΔK_d be {NB, NM, NS, ZO, PS, PM, PB}, representing {negative large, negative medium, negative small, zero, positive small, positive medium, positive large}, respectively. The affiliation functions are all selected as triangular functions. The controller model is constructed as shown in Figure 10, and the three-dimensional surfaces of the output quantities ΔK_p, ΔK_i, and ΔK_d on the theoretical domain are shown in Figure 11.
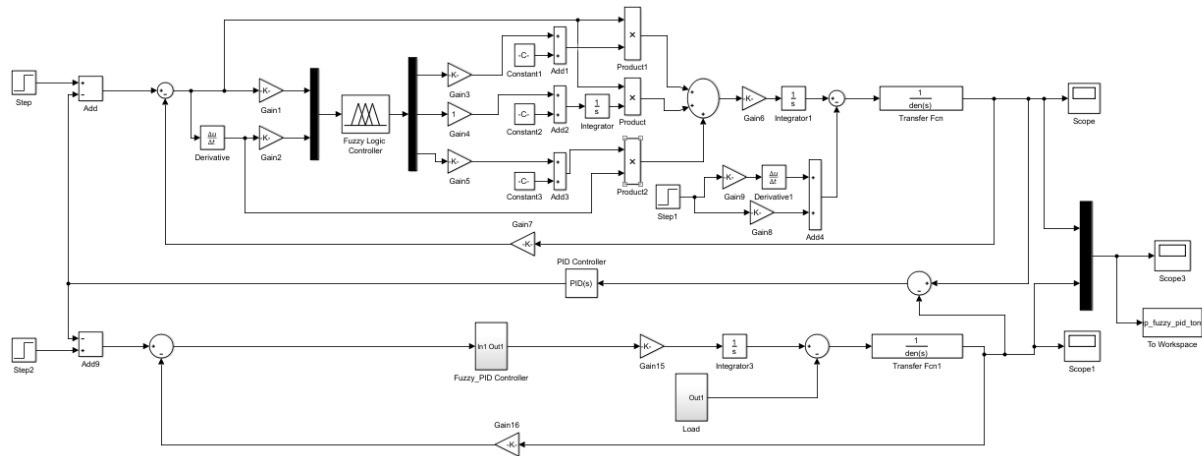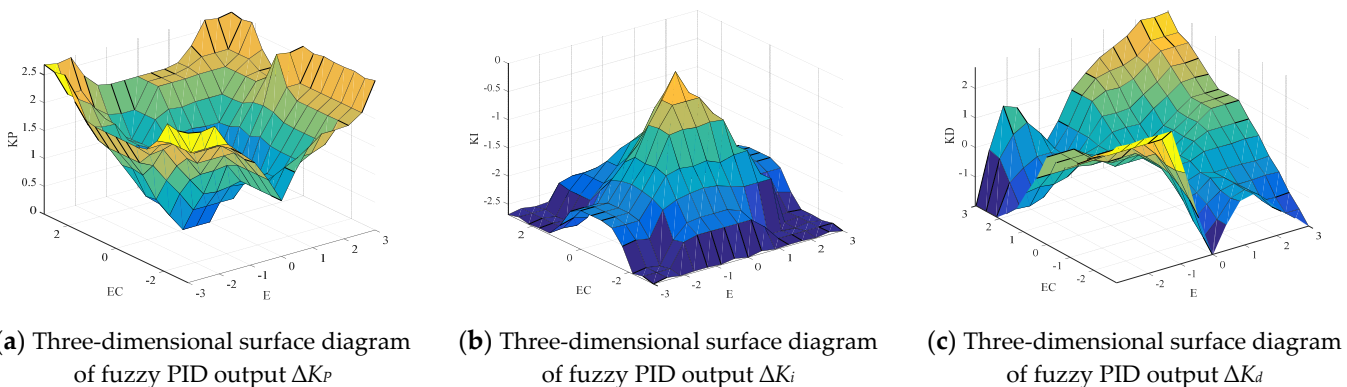

Figure 10. Fuzzy PID simulation model.

(**a**) Three-dimensional surface diagram of fuzzy PID output ΔK_P

(**b**) Three-dimensional surface diagram of fuzzy PID output ΔK_i

(**c**) Three-dimensional surface diagram of fuzzy PID output ΔK_d

Figure 11. Three-dimensional curved surface diagram of fuzzy PID output ΔK_P, ΔK_i and ΔK_d.

3.2.3. PID Parameter Self-Tuning Based on GA

In order to improve and optimize the PID parameters, a genetic algorithm optimization method was proposed to adjust the parameters of the PID controller in order to improve the stability, robustness, and fast response of the system.

A GA (Genetic Algorithm) begins a search from the string set of the problem with large coverage, and as it is a parallel search based on a chromatic population with a guessing nature of selection, replication, exchange, and mutation operations are used to evaluate multiple solutions in the search space in order to reach the optimal solution to a problem [17,18].

The GA self-tuning PID parameter design scheme used here was as follows:

(1)   Coding method and genetic operation

The encoding method used binary encoding strings of length 10 to represent the three decision variables, K_p, K_i, and K_d. The basic operations of the genetic algorithm were selection, crossover, and variation. In this paper, the selection operation used the

proportional selection operator, the crossover operation used the single-point crossover operator, and the variation operation used the basic bitwise variation operator.

(2) Selection of fitness function

Genetic algorithms generally do not require other external information in the search for evolution, and use fitness as a measure of individual merit in the population and as a basis for genetic manipulation. The selection of the fitness function depends on the objective function of the specific problem. In order to obtain a better dynamic response, the "absolute value of error time integral performance index" was used as the minimum objective function for PID parameter selection. The squared term of the control input was added to the objective function. The selected objective function is shown in the following equation:

$$J = \int_0^\infty (\omega_1 |e(t)| + \omega_2 u^2(t)) dt + \omega_3 t_u \tag{5}$$

where $e(t)$ is the system error, $u(t)$ is the output of the controller, t_u is the rise time, and ω_1, ω_2, ω_3 is the weight.

In order to avoid overshooting a penalty control was used in the operation process. When overshoot is generated, the amount of overshoot should be taken as one of the optimal indicators in the objective function, at which time the minimum objective function is as follows:

If

$$ey(t) < 0,$$
$$J = \int_0^\infty (\omega_1 |e(t)| + \omega_2 u^2(t) + \omega_4 |ey(t)|) dt + \omega_3 t_u \tag{6a}$$

Else

$$J = \int_0^\infty (\omega_1 |e(t)| + \omega_2 u^2(t)) dt + \omega_3 t_u \tag{6b}$$

where ω_4 is the weight value, $\omega_4 >> \omega_1$, $ey(t) = y(t) - y(t-1)$, and $y(t)$ is the actual output of the controlled object.

The minimum value of this objective function responds to the optimal value of the control system's error, energy, and response time. The adaptation function is selected as follows:

$$F = \frac{1}{J} \tag{7}$$

where J is the objective function adaptation value.

A change in the objective function is usually used to characterize the optimization process of the parameters during the self-tuning of the genetic algorithm PID parameters. The minimum value indicates the optimal individual of the PID parameters using binary encoding, while the value of the objective function corresponding to different control objects is different.

(3) Parameter tuning and optimization process

The parameter rectification and optimization search process was as follows: (1) determine the range of K_p, K_i, K_d and the coding length, then perform coding; (2) generate the initial population P_0; (3) decode the individuals in the population into the corresponding parameter values and use these parameters to find the objective function value J and fitness function F; (4) perform selection, crossover, and mutation operations on population P_0 to generate the next-generation population $P(t + 1)$; (5) repeat Steps (3) and (4) until a satisfactory value is reached. A flow chart is shown in Figure 12.
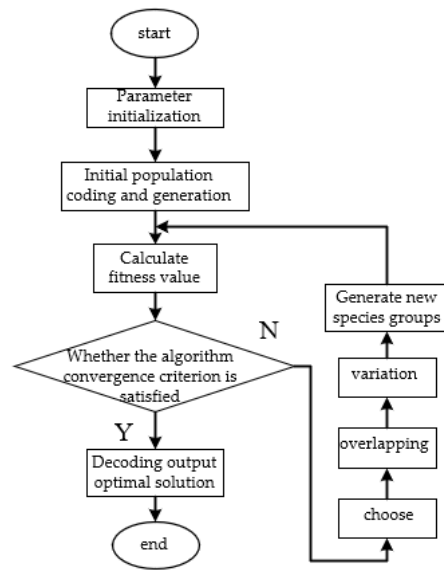
Figure 12. Flow chart of PID parameter self-tuning based on GA.

(4)   GA self-tuning PID parameter setting

Taking the front drive motor system of the hydraulic travel system as an example, before using the genetic algorithm to adjust the PID parameters of the system, it is necessary to determine the range of PID parameters to be adjusted according to the actual situation. The value ranges of PID parameters were K_p (0.0010, 30.0000), K_i (0.0010, 10.0000), K_d (0.0010, 10.0000), the initial population number was 30, and the number of population iterations was 100. For objective function weight selection, ω_1 = 0.9960, ω_2 = 0.0010, ω_3 = 2.0000, and ω_4 = 180.0000. The MATLAB program was used for operation simulation and the genetic algorithm is used to optimize the PID parameters of the control system. The simulation model was built in Simulink, as shown in Figure 13.
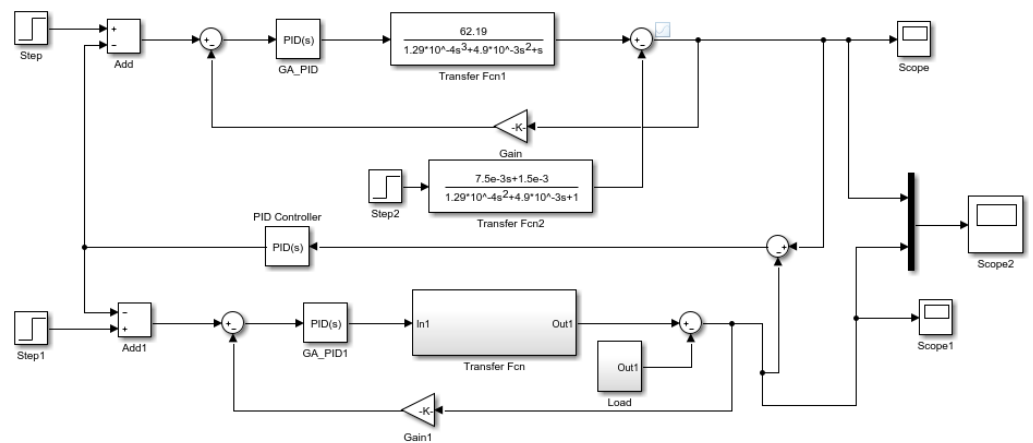

Figure 13. Genetic algorithm self-tuning PID simulation model.

3.2.4. Self-Tuning of PID Parameters Based on BP

A BP (Back-propagation) neural network is a multilayer feedforward network trained according to the error back-propagation algorithm, which mainly utilizes the gradient search technique of the gradient descent method to continuously adjust the weights and thresholds of the connections between network layers by back-propagation in order to minimize the sum of squared errors between the actual and desired outputs of the network and to make the system optimal by continuously adjusting the weights and thresholds between network layers [19,20] A typical three-layer feedforward BP neural network structure is shown in Figure 14.
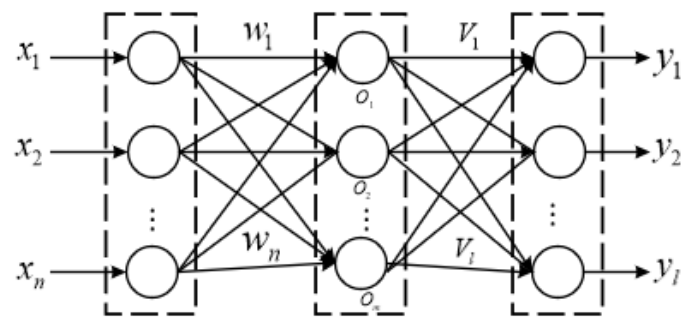
Figure 14. Typical feedforward BP neural network structure.

In a typical three-layer feed-forward BP neural network structure, the input vector is $X = (X_1, X_2, \ldots, X_n)$, the hidden layer vector is $O = (o_1, o_2, \ldots, o_m)$, the output vector is $Y = (y_1, y_2, \ldots, y_l)$, and the desired output vector is $D = (d_1, d_2, \ldots, d_l)$. The connection matrix between the input layer and the hidden layer is $W = (W_1, W_2, \ldots, W_j, \ldots, W_m)$ and the connection matrix between the hidden layer and the output layer is $V = (V_1, V_2, \ldots, V_k, \ldots, V_l)$. For the mathematical representation of the output layer,

$$y_k = f\left(\sum_{j=0}^{m} V_{jk}o_j\right) \quad k = 1, 2, \ldots, l \tag{8}$$

where, V_{jk} is the output layer matrix, O_j is the implied layer vector, and m, j is the number of connection matrices between the input layer and the hidden layer.

For hidden layer mathematical representation,

$$o_j = f\left(\sum_{i=0}^{n} W_{ij}x_i\right) \quad j = 1, 2, \ldots, m \tag{9}$$

where W_{ij} is the implied layer matrix and n is the number of implied layer matrices.

Where the transfer function $f(x)$ is a unipolar Sigmoid function,

$$f(x) = \frac{1}{1 + e^{-x}} \tag{10}$$

For each layer, the weight adjustment expression is

$$\begin{cases} \Delta W_{jk} = -\eta \frac{\partial E}{\partial W_{jk}} \\ \Delta V_{jk} = -\eta \frac{\partial E}{\partial V_{jk}} \end{cases} \quad (j = 1, 2, \ldots, m, \ k = 1, 2, \ldots, l) \tag{11}$$

where V_{jk} is the output layer matrix, W_{jk} is the matrix connecting the input layer to the implicit layer, and η is the learning rate coefficient.

When using a BP neural network to rectify the three parameters of the PID controller, it is necessary to determine the structure of the BP neural network, the initial values of the W_{ij} and output layer V_{jk} weighting coefficients, the learning rate, η, and the inertia coefficient, α. In this paper, the structure of the BP neural network was used for the 3-8-3 model. The initial value of the weighting coefficients of the implicit layer was $W_{ij} = 0.5$ rands (8,3), the initial value of the weighting coefficients of the output layer was $V_{jk} = 0.5$ rands (3,8), the learning rate was $\eta = 0.1000$, and the inertia coefficient was $\alpha = 0.0100$. Inertia coefficients were added to the BP neural network in order to avoid oscillations and slow convergence in the learning process of the weights. The controller parameters are varied, as shown in Figure 15; the controller builds the simulation model as shown in Figure 16 and the constant speed simulation model of the hydraulic travel system based on the neural network algorithm is shown in Figure 17.
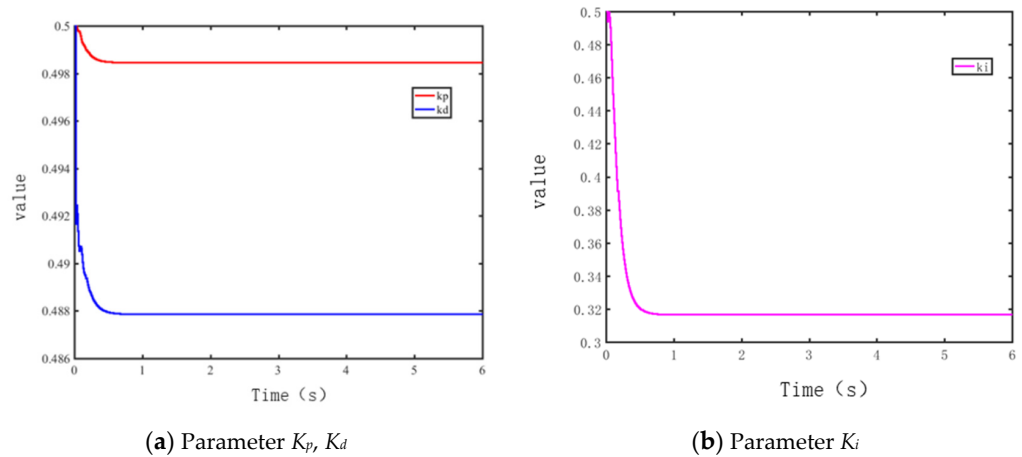
(**a**) Parameter K_p, K_d (**b**) Parameter K_i

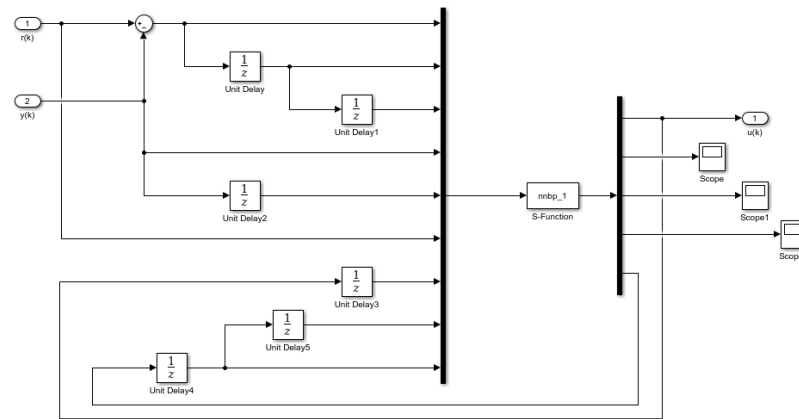**Figure 15.** BP_ Controller parameter variation curve.

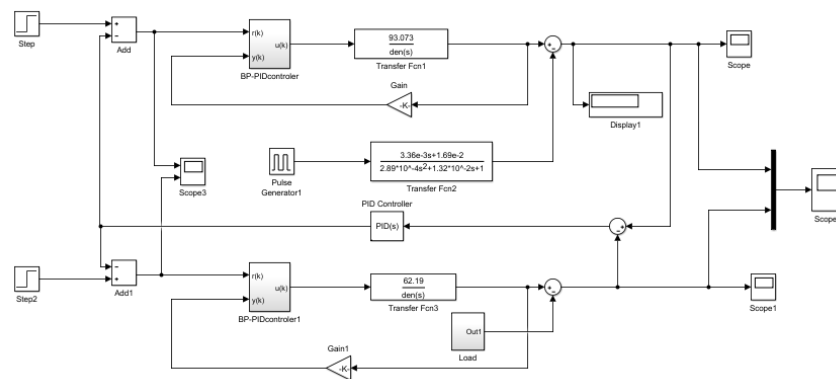**Figure 16.** BP_ Build simulation model of PID controller.

Figure 17. BP self-tuning PID simulation model.

4. Simulation Analysis

4.1. Constant Speed No-Load Simulation Analysis

Let the motor speed be 1600 r/min, the Amesim simulation time 30 s, and the Simulink simulation time 6 s. These were compared with a state machine using the statechart control module, Z–N frequency response PID control, fuzzy PID control, GA based PID control and BP algorithm based PID control. The simulation results of motor speed tracking under step signal were compared as well. As can be seen from Figure 18a, the maximum overshoot of the front-drive motor speed is 28.43% and the dynamic stabilization adjustment time is 8.3712 s under step signal simulation with the state machine statechart control method in Simcenter Amesim simulation software2019.1. The rear-drive motor has no overshoot, and

the dynamic stabilization adjustment time is longer, about 15.2528 s. It can be seen from Figure 18b that when using the PID control method based on Z–N frequency response, the maximum overshoot of the speed of the front drive motor is 9.38% and the dynamic stability adjustment time is 6.0746 s, the overshoot of the rear drive motor is 8.57%, and the dynamic stability adjustment time is about 5.0600 s. From Figure 18c, it can be seen that the maximum overshoot of the front motor speed is 1.69% and the dynamic stabilization time is about 1.2319 s with the fuzzy PID control method. The overshoot of the rear motor is 2.43% and the dynamic stability adjustment time is about 0.7524 s. As can be seen from Figure 18d, with the GA self-tuning PID control method there is no overshoot of the front motor and rear motor speed, and the dynamic stability adjustment time is 2.3800 s for the front motor and 0.6718 s for the rear motor. From Figure 18e, it can be seen that the PID parameter self-tuning control method based on BP algorithm has no overshoot in the speed of either the front drive motor or the rear drive motor, the dynamic stabilization adjustment time of the front drive motor is 1.5112 s, and the dynamic stabilization adjustment time of the rear drive motor is about 1.3910 s. The state machine with statechart control has a larger overshoot, and the synchronization speed time of the two motors is longer, thus, the dynamic response is poor. The Z–N frequency response PID control method has a better effect than the former one, however, at the same time there is a larger overshoot and longer dynamic response time. The overshoot and dynamic stable adjustment time of the fuzzy PID control method are better than the first two control methods, however, the dynamic adjustment is not smooth enough, which causes system oscillation during the rise. Both the GA self-tuning PID control method and BP algorithm PID parameter self-tuning control method have no overshoot, however, the time to reach synchronous speed of the double motors based on BP algorithm PID parameter self-tuning control is 36.55% shorter than GA self-tuning PID control, thus, the control effect is better.
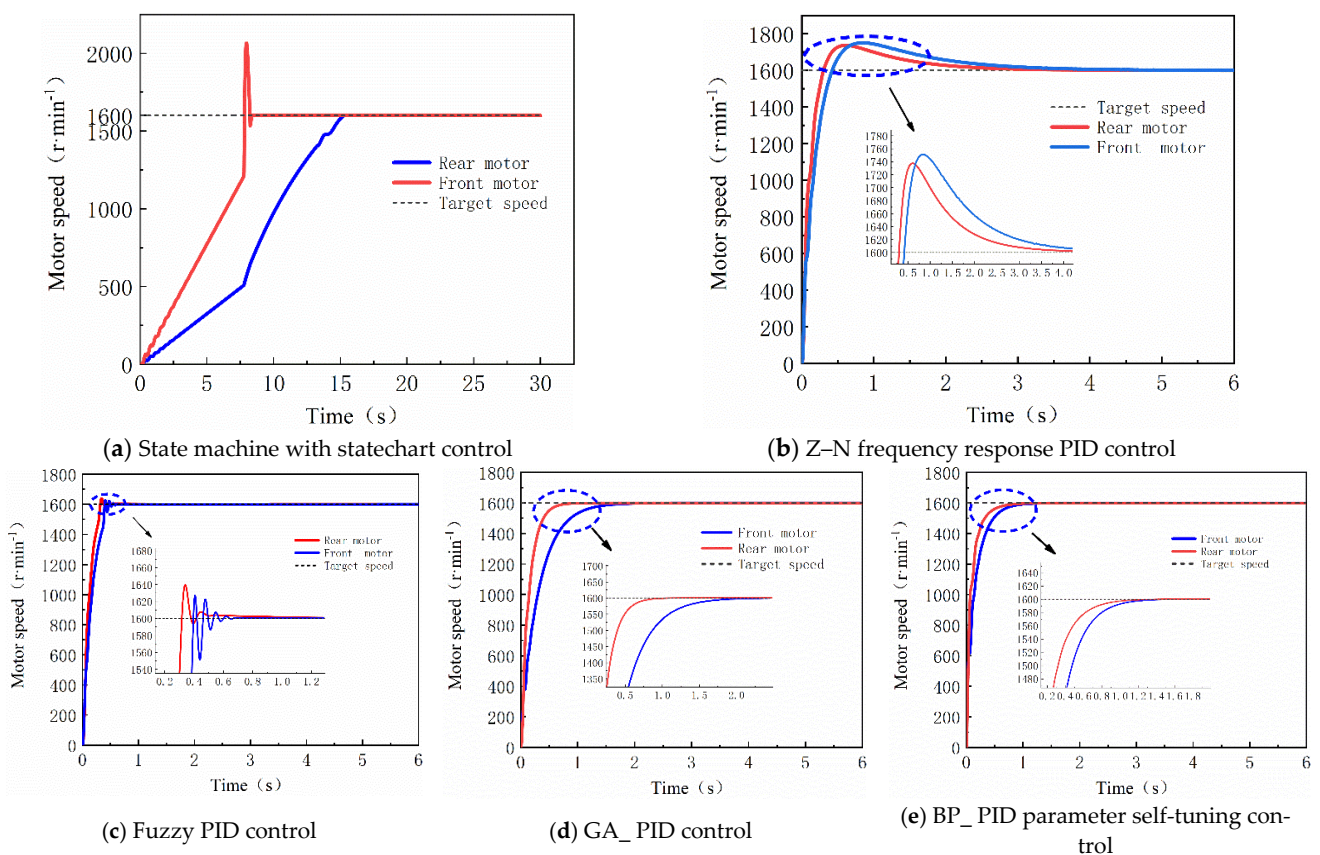

(**a**) State machine with statechart control

(**b**) Z–N frequency response PID control

(**c**) Fuzzy PID control

(**d**) GA_ PID control

(**e**) BP_ PID parameter self-tuning control

Figure 18. Design of adaptive tracking controller.

4.2. Constant Speed Load Simulation Analysis

With the simulation conditions otherwise unchanged, an external load signal of 400 N-m was added to the system at the 4th s. The simulation results are shown in Figure 19. After adding a 400N-m external load to the front drive motor, it can be seen that the maximum speed of the front drive motor decreases by 22 r/min using the PID parameter self-tuning control method based on BP algorithm, while the overshoot is 1.38%. The BP algorithm-based PID parameter self-tuning control method decreased by 4.20%, 2.32%, and 0.63%, respectively, compared to the Z–N frequency response PID-based control method, the PID control method using fuzzy PID, and the GA self-tuning PID control method, and the target speed could be tracked in about 0.2700 s. The rear drive motor decreased by a maximum of 46 r/min, while the overshoot is 2.88%, which is 3.00%, 0.31%, and 1.92% lower, respectively, than the first three control methods. Our analysis shows that system stability is better when using the PID parameter self-tuning control method based on the BP algorithm.
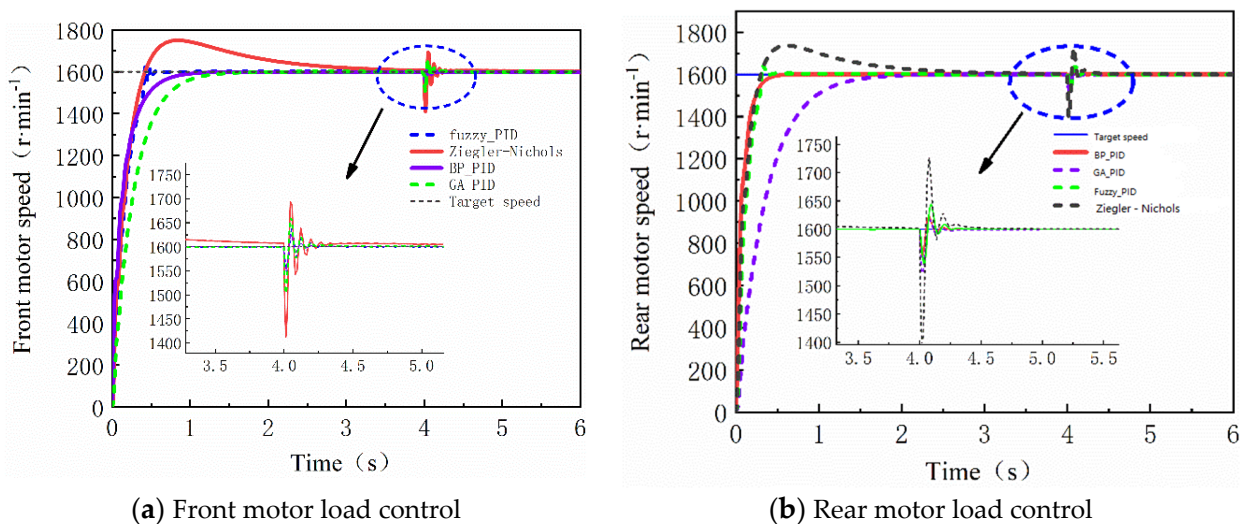

(**a**) Front motor load control   (**b**) Rear motor load control

Figure 19. System constant speed load control.

4.3. Motor Speed Synchronization Simulation Analysis

As shown in Table 2 and Figure 20, the Z–N frequency response PID control process has an overshoot amount, which causes system oscillation during the working process; the two motors take a long time to track the target speed synchronously. While the dynamic response of the fuzzy PID control system is fast, the system oscillation is more serious from zero to the target speed stage, and the hydraulic system does not work smoothly. The PID parameter self-tuning control based on BP algorithm has no overshoot, the two motors synchronously reach the target speed in a shorter time, and the hydraulic system works smoothly and stably. In the case of alternating and variable loads, the system remains stable and quickly synchronizes with the target speed. This analysis shows that system stability and synchronization are better with the PID parameter self-tuning control method based on the BP algorithm.

Table 2. Comparison of parameters of different control methods.

Parameter	Overshoot	Tracking Target Speed Time (s)
Ziegler-Nichols	9.25%	6.0746
Fuzzy_PID	2.38%	1.2319
BP_PID	none	1.5112

(**a**) Synchronous control of motor speed with different algorithms

(**b**) Synchronous control of motor speed alternating load based on BP algorithm
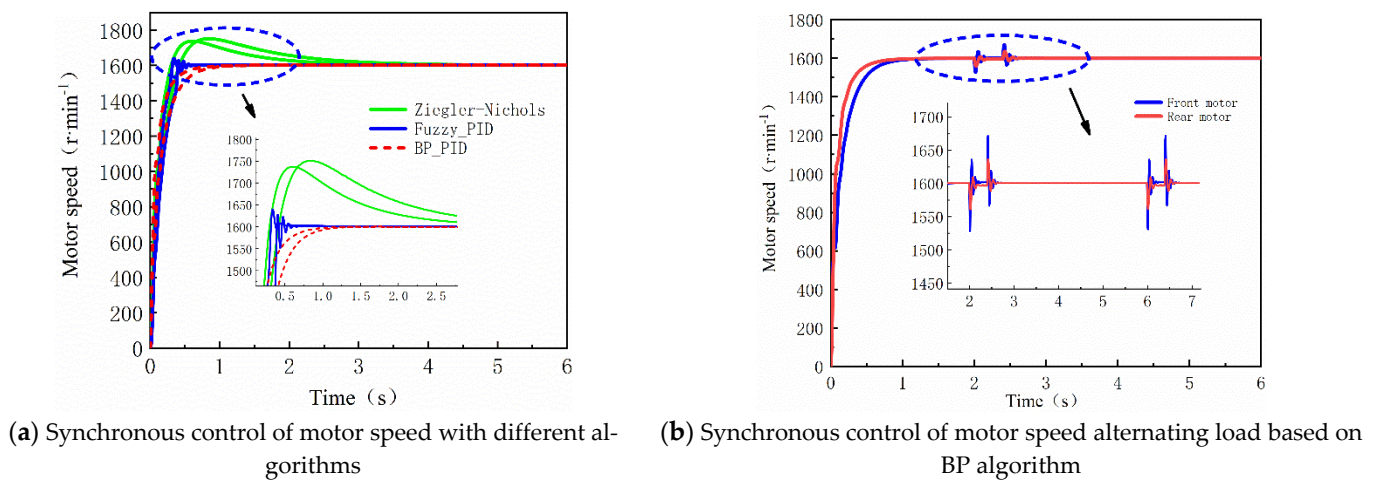
Figure 20. Synchronous control of motor speed.

5. Discussion

Under constant speed no-load operating conditions, the state machine with statechart control has a larger overshoot, the synchronization speed time of the two motors is longer, and the dynamic response is poor. The Z–N frequency response PID control method has a better effect than the former one; however, at the same time it has a larger overshoot and longer dynamic response time. The overshoot and dynamic stable adjustment time of the fuzzy PID control method are better than the first two control methods; however, the dynamic adjustment is not smooth enough, which causes system oscillation during the rise. While the GA self-tuning PID control method and the BP algorithm PID parameter self-tuning control method both have no overshoot, the time needed to reach synchronous speed of the double motors based on the BP algorithm PID parameter self-tuning control is 36.55% shorter than the GA self-tuning PID control, thus, the control effect is better.

Under constant speed and variable load conditions, the Z–N frequency response PID control process has an overshoot amount, which causes system oscillation during the working process, and the two motors require a long time in order to track the target speed synchronously. While the dynamic response of the fuzzy PID control system is fast, the system oscillation is more serious from zero to the target speed stage, and the hydraulic system does not work smoothly. On the other hand, the PID parameter self-tuning control based on the BP algorithm has no overshoot, the two motors synchronously reach the target speed in a shorter time, and the hydraulic system works smoothly and stably.

6. Conclusions

Aiming to eliminate instability and synchronize motor speed under step input speed and external load disturbance conditions, the research object of this paper was a hydraulic travel system with a single pump and double motors. Based on the establishment of its mathematical model, a variety of different control strategies were proposed for analysis and comparison. The conclusions are as follows:

1. In this paper, five different control strategies were designed and each control strategy was compared and analyzed. The PID parameter self-tuning control method based on a BP algorithm was determined to realize the best constant control of the system output speed.
2. In no-load, load, and multi-alternating load cases, the PID parameter self-tuning control method based on BP algorithm had the smallest speed overshoot of both the front-drive and rear-drive motor and the shortest dynamic stability adjustment time. The dynamic response effect was better and the hydraulic system was more smooth and more stable.

3. The PID parameter self-tuning control method based on BP algorithm required a shorter time for the two motors to reach the target speed synchronously, and the working process of the hydraulic system was smooth and stable compared to the other control methods. Under sudden changes and changeable loads, the system remained stable and quickly synchronized with the target speed.

The designed hydraulic travel system with a PID parameter self-tuning controller based on a BP algorithm is able to output the speed of the dual hydraulic motors in a constant and synchronous manner under the conditions of sudden and variable loads and step input speed. These results help to obtain new insights and provide a reliable method for improving the existing hydraulic systems of engineering and agricultural machinery.

Author Contributions: Conceptualization, H.Y. and X.N.; methodology, H.Y.; software, H.Y.; validation, H.C., D.L. and W.P.; formal analysis, H.Y.; investigation, H.Y.; resources, X.N.; data curation, X.N.; writing—original draft preparation, H.Y.; writing—review and editing, H.Y.; visualization, H.C.; supervision, X.N.; project administration, H.Y.; funding acquisition, X.N. All authors have read and agreed to the published version of the manuscript.

Institutional Review Board Statement: Not applicable.

Informed Consent Statement: Not applicable.

Data Availability Statement: All relevant data presented in the article are stored according to institutional requirements and, as such, are not available online. However, all data used in this Manuscript can be made available upon request to the authors.

Conflicts of Interest: The authors declare no conflict of interest.

References

1. Lapinskas, A.; Kirka, A.; Lapinskas, R. Analysis of hydro motor velocity stabilization. *Elektron. Elektrotechnika* **2008**, *81*, 57–60.
2. Bennett, J.M.; Roberton, S.D.; Jensen, T.A.; Antille, D.L.; Hall, J. A comparative study of conventional and controlled traffic in irrigated cotton: I. Heavy machinery impact on the soil resource. *Soil Tillage Res.* **2017**, *168*, 143–154. [CrossRef]
3. Vardhan, A.; Dasgupta, K.; Kumar, N. Comparison of the steady-state performance of hydrostatic drives used in the rotary head of the drill machine. *J. Braz. Soc. Mech. Sci. Eng.* **2017**, *39*, 4403–4419. [CrossRef]
4. Stump, P.; Keller, N.; Vacca, A. Energy Management of Low-Pressure Systems Utilizing Pump-Unloading Valve and Accumulator. *Energies* **2019**, *12*, 4423. [CrossRef]
5. Ciurys, M.P.; Fiebig, W. Experimental Investigation of a Double-Acting Vane Pump with Integrated Electric Drive. *Energies* **2021**, *14*, 5949. [CrossRef]
6. Zhu, C.H.; Zhang, H.M.; Wang, W.Z.; Li, K.; Zhou, Z.; He, H. Compound Control on Constant Synchronous Output of Double Pump-Double Valve-Controlled Motor System. *Processes* **2022**, *10*, 528. [CrossRef]
7. Backas, J.; Ghabcheloo, R. Nonlinear model predictive energy management of hydrostatic drive transmissions. *Proc. Inst. Mech. Eng. Part I J. Syst. Control. Eng.* **2019**, *233*, 335–347. [CrossRef]
8. Paszota, Z. Graphical presentation of the power of energy losses and power developed in the elements of hydrostatic drive and control system Part II Rotational hydraulic motor speed parallel throttling control and volumetric control systems. *Pol. Marit. Res.* **2008**, *15*, 21–29. [CrossRef]
9. Kazama, E.H.; da Silva, R.P.; Ormond, A.T.S.; Alcantara, A.S.; do Vale, W.G. Cotton and fiber quality in function of picker harvest speed. *Rev. Bras. Eng. Agr. Amb.* **2018**, *22*, 583–588. [CrossRef]
10. Hasan, M.E.; Ghoshal, S.K.; Dasgupta, K.; Kumar, N. Dynamic analysis and estimator design of a hydraulic drive system. *J. Braz. Soc. Mech. Sci. Eng.* **2017**, *39*, 1097–1108. [CrossRef]
11. Shouran, M.; Alsseid, A. Particle Swarm Optimization Algorithm-Tuned Fuzzy Cascade Fractional Order PI-Fractional Order PD for Frequency Regulation of Dual-Area Power System. *Processes* **2022**, *10*, 477. [CrossRef]
12. Rocha, E.M.; Junior, W.B.; Bezerra, A.C.S.; Barra, H.M. Preventing Damage in Hydraulic Pumping Systems by using a Pressure Control Strategy. *IEEE Lat. Am. Trans.* **2017**, *15*, 445–453. [CrossRef]
13. Lin, C.; Sun, S.; Walker, P.; Zhang, N. Off-Line Optimization Based Active Control of Torsional Oscillation for Electric Vehicle Drivetrain. *Appl. Sci.* **2017**, *7*, 1261. [CrossRef]
14. Paszota, Z. The operating field of a hydrostatic drive system parameters of the energy efficiency investigations of pumps and hydraulic motors. *Pol. Marit. Res.* **2009**, *16*, 16–21. [CrossRef]

15. Rossetti, A.; Macor, A.; Benato, A. Impact of control strategies on the emissions in a city bus equipped with power-split transmission. *Transp. Res. Part D Transp. Environ.* **2017**, *50*, 357–371. [CrossRef]
16. Li, X.; Zhao, L.; Zhou, C.; Li, X.; Li, H. Pneumatic ABS Modeling and Failure Mode Analysis of Electromagnetic and Control Valves for Commercial Vehicles. *Electronics* **2020**, *9*, 318. [CrossRef]
17. Zhao, X.; Ni, X.D.; Wang, Q.; Bao, M.X.; Li, S.; Han, S.M. Research on adaptive control strategy of hydraulic mechanical continuously variable transmission of a cotton picker. *Proc. Inst. Mech. Eng. Part C J. Mech. Eng. Sci.* **2020**, *234*, 3335–3345. [CrossRef]
18. Wei, X.; Wang, L.; Ni, X.; Han, S.; Zhao, X.; Li, S. Speed control strategy for pump-motor hydraulic transmission subsystem in hydro-mechanical continuously variable transmission. *J. Mech. Sci. Technol.* **2021**, *35*, 5665–5679. [CrossRef]
19. Ghoshal, S.K.; Pandey, A.K.; Dasgupta, K.; Bhola, M. A segmental pump-motor control scheme to attain targeted speed under varying load demand of a hydraulic drive used in heavy earth movers. *Mechatronics* **2021**, *80*, 102681. [CrossRef]
20. Baker, K.D.; Hughs, E.; Foulk, J. Spindle Speed Optimization for Cotton Pickers. *Appl. Eng. Agric.* **2015**, *31*, 217–225.